International Journal of Automotive Technology, Vol. 13, No. 1, pp. 43−60 (2012)
DOI 10.1007/s12239−012−0005−8

1229−9138/2012/062−05

DYNAMIC HARDENING EQUATION OF THE AUTO-BODY STEEL SHEET WITH THE VARIATION OF TEMPERATURE

H. HUH[1)*], H. J. LEE[2)] and J. H. SONG[3)]

[1)]School of Mechanical, Aerospace and Systems Engineering, KAIST, Daejeon 305-701, Korea
[2)]Structure Research Departments, Hyundai Heavy Industries Co., Jeonha-dong, Dong-gu, Ulsan 682-792, Korea
[3)] Department of Manufacturing Convergence Technology, Korea Institute of Industrial Technology, 1271-18 Sa-3 dong, Sangrok-gu, Ansan-si, Gyeonggi 426-173, Korea

(Received 22 September 2011; Revised 12 October 2011)

ABSTRACT−This paper is concerned with the empirical hardening equation of steel sheets for an auto-body at intermediate strain rates with the variation of temperature. In order to identify the temperature dependence of the strain-rate sensitivity of steel sheets such as SPRC35R, SPRC45E and TRIP60, uniaxial tensile tests have been performed with the variation of the strain rate from 0.001/sec to 200/sec and the environmental temperature from –40ºC to 200ºC. The thermo-mechanical response at the quasi-static state is obtained from static tensile tests and that at the intermediate strain rate is obtained from high speed tensile tests. The effects of both the strain rate and the temperature on the flow stress and the fracture elongation are investigated with the experimental data. Experimental results provide the variation of the strain-rate sensitivity with respect to the temperature. They also show that as the strain rate increases, the variation of flow stress becomes sensitive to the temperature. A phenomenological constitutive model is newly proposed by modifying the well-known Khan–Huang–Liang model. Based on the experimental data, both the strain rate and the temperature dependent sensitivity of the flow stress are considered in the proposed model by coupling the strain, the strain rate and the temperature. In order to verify the accuracy of the proposed model quantitatively, the standard error between the experimental data and the fitted one is compared with other empirical constitutive models such as the Johnson–Cook and the Khan–Huang–Liang models. The comparison demonstrates that the model proposed gives relatively accurate description of the experimental data at the various strain rates and temperatures.

KEY WORDS : Constitutive model, Dynamic thermo-mechanical response, Strain-rate sensitivity, Temperature sensitivity, Intermediate strain rate

1. INTRODUCTION

The recent megatrend of both automobile users and industries is to demand better vehicle safety and crashworthiness although the light weight design for the reduction of fuel consumption becomes a very challenging issue. Confronting these contradictory requirements, design of a light weight vehicle with enhanced crashworthiness needs to seek for an optimum combination of body structures and materials (Porsche Engineering Service Inc., 2001; Huh *et al*., 2003; Kim *et al.*, 2006). Advances in the computational technology and finite element method make it feasible to consider both the crashworthiness and the weight of the body structure in the early stage of auto-body design. Most automotive companies now utilize CAE to perform virtual crash tests on computers. Engineers can quickly adjust the structural performance before performing a real crash test to accomplish the light weight vehicle with enhanced crashworthiness (Tateno *et al*., 1998; Kim and Huh, 2006). In this procedure, the accuracy of crash analysis becomes important to guarantee the reliability of the auto-body design (Yasuki, 2000; Huh and Kang, 2002; Song *et al*., 2006). Reliable crash simulation necessitates an adequate physical and numerical modeling of the mechanical behavior of auto-body materials considering both the strain rate and the temperature (Meyers, 1994). Particularly, the material properties of steel sheets are important to the car crash because more than 70% of the auto-body is composed of steel sheets.

Plastic deformation of steels and other metals is sensitive to the strain rate and the temperature at which the deformation is taking place (Zener and Holloman, 1944; Hoge and Mukherjee, 1977; Zukas *et al.*, 1982; Robert, 1983). The effect of the strain rate and the temperature on the response of steels has been examined in many investigations by Campbell and Ferguson (1970), McCormick (1978), Costin *et al*. (1979), Eleiche (1981) and Klepaczko and Duffy (1982). They used different techniques by modifying split Hopkinson bar apparatus, which is also called Kolsky's apparatus (Kolsky, 1949), in order to perform

**Corresponding author*. e-mail: hhuh@kaist.ac.kr

tests for various compositions of mild steel over a wide range of strain rates and temperatures. Ishikawa and Tanimura (1992) examined the strain-rate sensitivity of flow stress for 304N stainless steel at strain rates between 10^{-3}/sec and 1000/sec at low temperatures ranging from 83K to 296K using torsional Hopkinson bar test. Gilat and Wu (1997) studied the response of a hot-rolled 1020 steel at the strain rates 5×10^{-4}/sec, 2/sec and 1000/sec with various temperatures ranged from 25°C to 600°C. Khan and Liang (1999, 2000) studied the dynamic behaviors of three BCC metals of tantalum, tantalum alloy and AerMet 100 steel over a range of strain rates from 10^{-6}/sec to 10^{4} /sec and temperatures from 77°F to 600°F. Netmat-Nasser and Guo (2001, 2003) performed Hopkinson bar tests with AL-6XN stainless steel, DH-36 structural steel for ships and Nitronic-50 stainless steel over a wide range of temperatures from 77K to 1000K and they used to address the dynamic and the thermal softening behavior of these steels at high strain rate deformation. Lee and Liu (2006) conducted a compressive type Hopkinson bar test in order to compare the dynamic behavior of three steels with different levels of carbon content under strain rates ranging from 1.1×10^{3}/sec to 5.5×10^{3}/sec and temperatures ranging from 25°C to 600°C. Some studies on the dynamic behavior of the structural steel sheets for an auto-body at high strain rates above 1000/sec are conducted at room temperature (Shi and Meuleman, 1992; Miura *et al.,* 1996; Mahadevan *et al.*, 1998; Huh *et al.*, 2002). Although each investigation focused on a different aspect of testing methods or material responses, common characteristics observed were effects of strain rates and temperatures. Experimental results show that the flow stress required for plastic deformation decreases generally with increasing temperature and decreasing strain rate. An exception to this response is sometimes mentioned at some narrow range of temperatures where the stress increases with increasing temperature and decreasing strain rate. Such behavior is explained by dynamic strain aging (Cottrell, 1953; McCormick, 1978; Li and Leslie, 1978; Robinson and Shaw, 1994; Netmat-Nasser and Guo, 2001, 2003). Its main effects, other than negative strain-rate sensitivity, are increasing strain hardening, decreases in ductility, and jerky flow.

In a real auto-body crash, the range of the strain rate is several tens to hundreds per second under 500/sec. Although the steel sheets have been the subject of extensive studies both experimentally and theoretically in the past few decades, there are relatively little studies about the dynamic behavior of the steel sheets for an auto-body at the range of intermediate strain rates under 1000/sec considering the effect of the environmental temperature due to experimental difficulties. Huh *et al.* (2008, 2009) made a servo-hydraulic type high speed material testing machine and conducted dynamic tensile tests of seventeen different steel sheets for an auto-body at the intermediate strain rates ranging from 0.003/sec to 200/sec in order to investigate the effect of the strain rate on the flow stress and the failure elongation at room temperature.

Accurate modeling of the deformation process of materials with the variation of strain rate and temperature requires a reliable constitutive description of the stress–strain relation. Several constitutive relations have been proposed for the use in computational mechanics under high strain rate deformation. The constitutive models can be classified into two categories: the phenomenological models; and the physically-based models (Khan *et al*., 2004). The phenomenological models such as the Cowper–Symonds model (Cowper and Symonds, 1957), the Johnson–Cook model (Johnson and Cook, 1983), the modified Johnson–Cook model (Kang *et al.*, 1999) and the Khan–Huang–Liang model (Khan and Huang, 1992; Khan and Liang, 1999, 2000; Khan and Zhang, 2000) were based on the available experimental observation, while the physically-based models such as the Zerilli–Armstrong model (Zerilli and Armstrong, 1987), the mechanical threshold stress (MTS) model (Follansbee and Kocks, 1988) were developed based on the microscopic dislocation mechanism of plastic deformation. Some physically-based models were also suggested based on correlation of dislocation dynamics, thermally activated dislocation motion and dislocation drag mechanics (Nemat-Nasser and Isaacs, 1996; Gilat and Wu, 1997; Nemat-Nasser *et al.*, 2001; Uenishi and Teodosiu, 2004; Abed and Voyiadjis, 2005).

Since the physically-based models have many material constants and difficulties for using in computational procedures, the phenomenological models are widely utilized in the finite element crash simulation. However, these phenomenological models are based on the experimental data obtained from the Hopkinson bar test at high strain rates. The flow stress at the intermediate strain rate ranged from 1/sec to 200/sec is just estimated by interpolating the flow stress obtained from the quasi-static test and the high strain rate test. It is evident that this interpolation scheme is not able to accurately describe the variation of the flow stress at the range of intermediate strain rates.

This paper deals with the study of the thermo-mechanical response of the steel sheets for an auto-body at the intermediate strain rate ranged from 1/sec to 200/sec. The objective is to obtain a complete set of experimental data with the variation of strain rate and temperature and utilize it for developing the phenomenological constitutive equation that can describe both the strain rate and the temperature dependent stress–strain curves. In order to identify the temperature dependent dynamic response of the steel sheets for an auto-body such as SPRC35R, SPRC45E and TRIP60, uniaxial tensile tests have been performed with the variation of strain rate from 0.001/sec to 200/sec and the variation of the environmental temperature from –40°C to 200°C. The thermo-mechanical response at the quasi-static state is obtained with the static tensile test and that at the intermediate strain rate is

obtained with high speed tensile tests. From the tensile test, the dynamic material behavior such as the flow stress, fracture elongation, the strain rate and temperature sensitivity of the flow stress are investigated quantitatively with the variation of strain rate and temperature. Quantitative comparison of both the strain-rate sensitivity and the temperature sensitivity of the flow stress are also performed in order to investigate the effect of the strength of material on the thermo-mechanical response. Based on the experimental data, a new constitutive relationship is proposed for modeling the material behavior over the whole testing range. The Khan–Huang–Liang model is modified to take account of both the strain rate and the temperature dependent sensitivity of the flow stress by coupling the strain, the strain rate and the temperature. In order to verify the accuracy of the proposed model quantitatively, the standard error (Stevenson, 1982) between the experimental data and the interpolated one is compared with other well-known constitutive models such as the Johnson–Cook model and the Khan–Huang–Liang model. The comparison demonstrates that the model proposed gives the relatively accurate description of the experimental data at various temperatures and intermediate strain rates.

2. EXPERIMENTAL DETAILS

Tensile tests were performed at the strain rate ranged from 0.001/sec to 200/sec and the temperature ranged from –40°C to 200°C in order to obtain the thermo-mechanical behavior of SPRC35R, SPRC45E and TRIP60 which is widely used for structural members of an auto-body. The thermo-mechanical response at the strain rate of 0.001/sec is obtained using the Instron hydraulic testing machine, Instron 4206, with an environmental chamber. For the dynamic tensile test at the intermediate strain rate up to the strain rate of 200/sec, a servo-hydraulic high speed material testing machine was utilized (Huh *et al*., 2008, 2009). The machine has a maximum stroke velocity of 7800 mm/s, a maximum load of 30 kN and a maximum displacement of 300 mm with a maximum hydraulic pressure of 300 bars and a maximum flow rate of 240 litre/min.

During the operation of the high speed material testing machine, a function generator transmits an input signal to the servo controller to control the displacement with a feed back system by comparing the measured displacement with the input signal. For the high speed tensile test, the load cell must have good response in the dynamic motion since material testing at the intermediate strain rate lasts only for several milli-seconds. The machine equipment is set up with the Kistler 9051A piezo-electric type load cell in a specially designed loading fixture to reduce the noise level and to increase the noise frequency in the load–displacement curve. The machine is well calibrated. Configuration file and test programs are fine tuned for different velocity of a stroke at different strain rates. Several experiments were

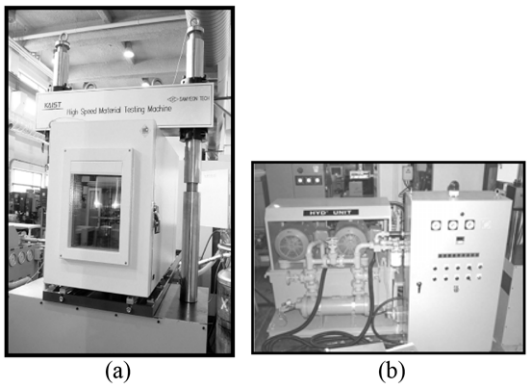

Figure 1. High speed material testing machine: (a) frame of the machine with a chamber; (b) hydraulic unit.

conducted at the same condition to verify repeatability and the results were very repeatable indicating that the machine response, testing procedure and material response were consistent. The environmental chamber is also equipped for the dynamic material tests with various temperatures ranged from –50°C to 350°C. Elevated temperatures are attained by radiant-heating with a quartz-lamp while low temperatures are obtained with a liquid nitrogen gas. The temperature is measured using a thermocouple arrangement. The temperature is maintained constant to within ±1°C. The high speed material testing machine used in the experiments are shown in Figure 1.

Tensile specimens for the standard test are specified with the regulation of ASTM, JIS and KS as well as the testing method. The regulation, however, does not include the high speed tensile testing method and the corresponding specimens. An appropriate specimen, thus, needs to be determined for accurate tensile tests with the machine developed at the intermediate strain rate. The dimensions of a specimen were selected from finite element analysis results with the Johnson–Cook model considering the shape factors such as gauge length, width and fillet radius to induce uniform deformation in the gauge region at the intermediate strain rate (Huh *et al.*, 2008). Considering the effect of shape factors, the dimensions of a tensile specimen were determined as shown in Figure 2. Uniform deformation was observed in the region of the gauge length

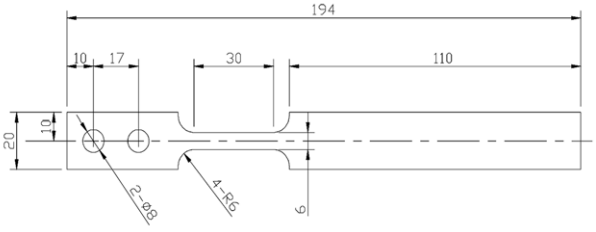

Figure 2. Dimension of a specimen for tensile tests at intermediate strain rates.

Table 1. Chemical composition of SPRC35R, SPRC45E and TRIP60.

Material	Chemic composition [wt %]					
	C	Si	Mn	P	S	Al
SPRC35R	0.04	0.03	0.50	0.035	0.025	0.045
SPRC45E	0.0016	0.0084	1.573	0.113	0.006	0.045
TRIP60	0.0996	1.165	1.373	0.022	0.003	0.039

without deformation concentration as results of both finite element analyses and experiments.

SPRC35R, SPRC45E and TRIP60 were tested along the rolling direction at the strain rate of 0.001, 0.1, 1, 10, 100 and 200/sec over a range of temperatures from –40ºC 200ºC considering the operating temperature of an auto-body. From the tensile test, the dynamic material behavior such as the flow stress, the strain-rate sensitivity and the temperature sensitivity of the flow stress are investigated quantitatively with the variation of strain rates and temperatures. The chemical compositions of the three steel sheets investigated in the present study are explained in Table 1.

3. EXPERIMENTAL RESULTS AND DISCUSSION

3.1. Strain Rate and Temperature Sensitivity

The stress–strain curves of steel sheets at various strain rates and the corresponding temperatures are obtained from the experiments as shown in Figure 3, 4 and 5, respectively. The experimental data indicates that the material response changes significantly with respect to the variation of strain rate and temperature. The strain-rate dependence of the flow stress and the work hardening behavior can be observed in the experimental data. Figures explain that the yield strength increases significantly but the slope of the stress–strain curve for strain hardening decrease as the strain rate increases. As a result, the ultimate tensile strength occurs at the lower strain and the hardening exponent becomes smaller with the increase of the strain rate. These results reveal that the flow stress shows the positive strain-rate sensitivity while the work hardening shows the negative sensitivity with respect to the strain rate. It can be also seen that the flow stress and the work hardening behavior are very much dependent on the temperature. This phenomenon seems to occur with the mechanism of grain sliding and the heat dissipation from the plastic work at intermediate strain rates. Temperature has a significant effect on the flow stress of metals. As the temperature increases, the dislocation movement occurs more rapidly and hence the resistance of the material to deformation decreases. Consequently, the flow stress is decreased as the environmental temperature increases as shown in figures. Figures also represents that the amount of increase in the

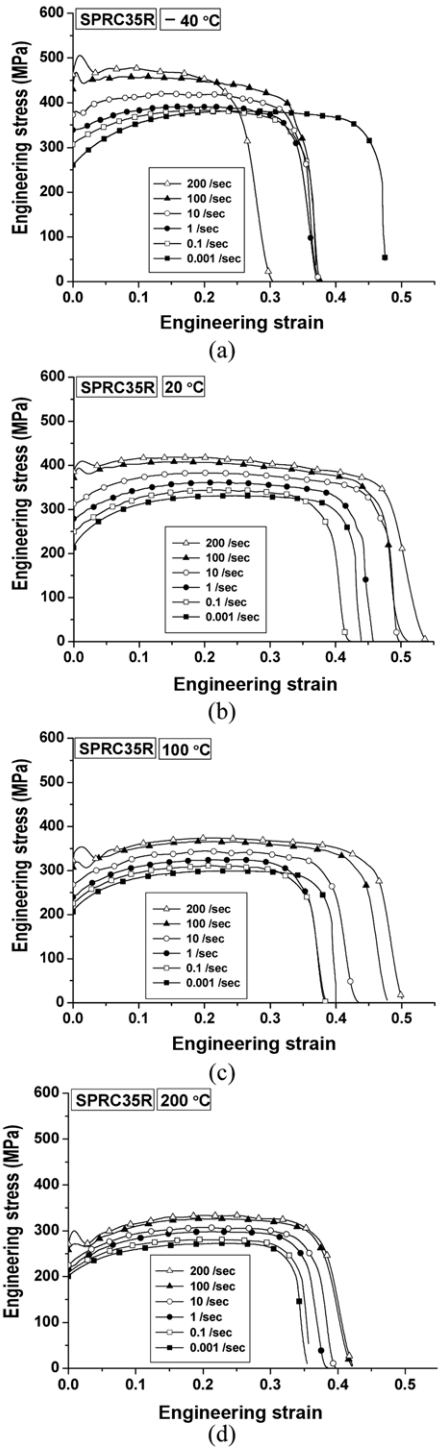

Figure 3. Engineering stress–strain curves of SPRC35R with the variation of the strain rate and the temperature: (a) –40ºC; (b) 20ºC; (c) 100ºC; (d) 200ºC.

flow stress with respect to the increase of strain rate, which is called as the strain-rate hardening, becomes large with the temperature elevation.

The stress–strain curves obtained in the experiment

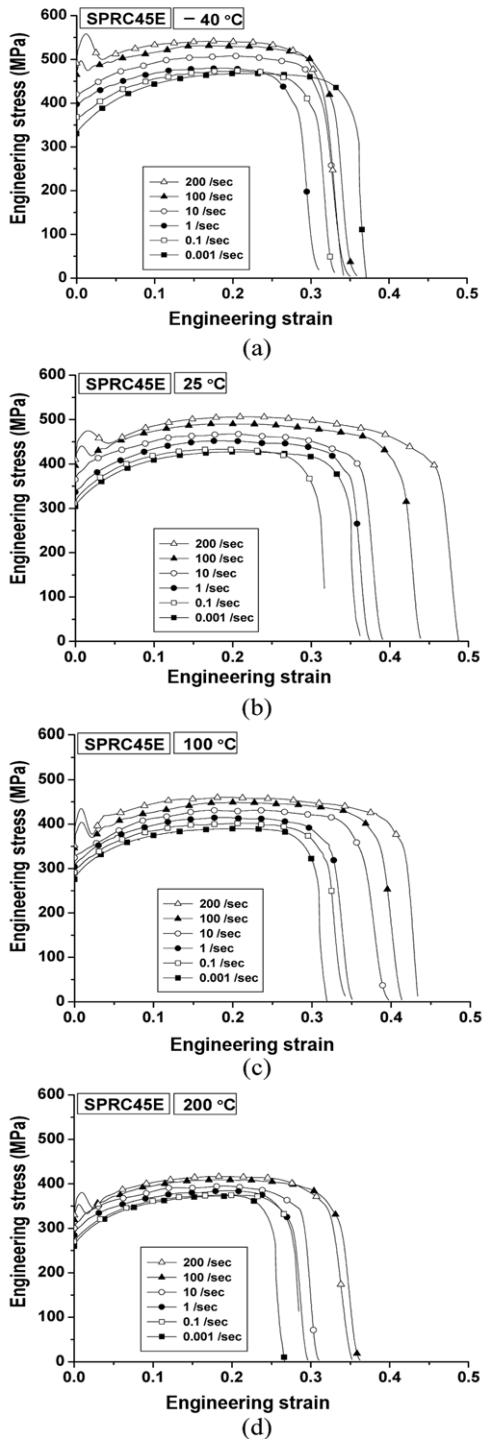

Figure 4. Engineering stress–strain curves of SPRC45E with the variation of the strain rate and the temperature: (a) –40ºC; (b) 25ºC; (c) 100ºC; (d) 200ºC.

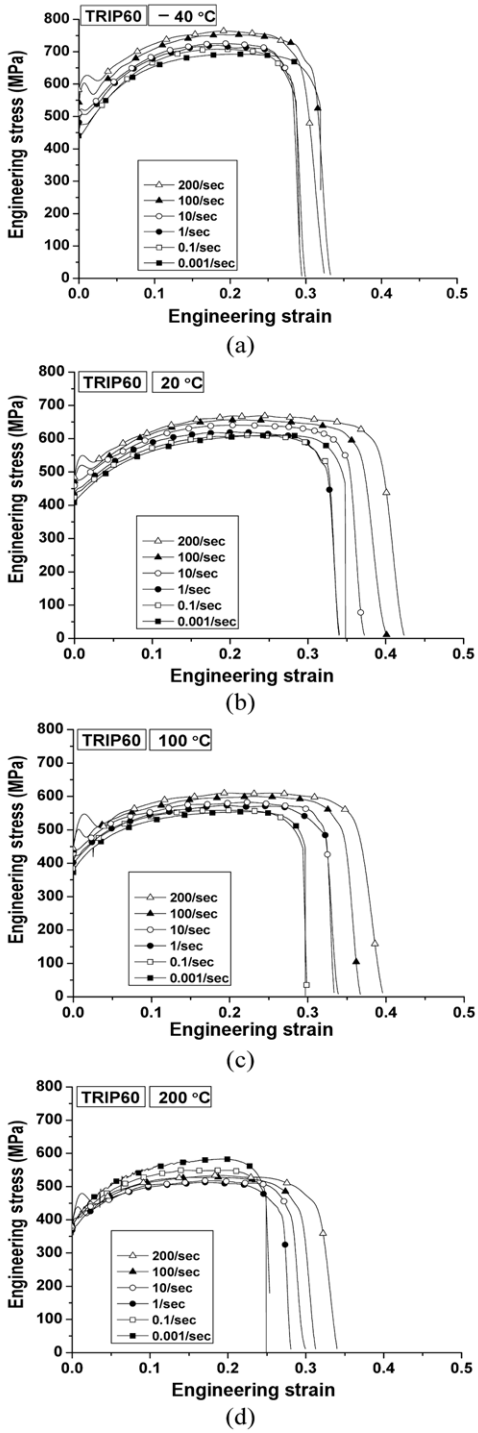

Figure 5. Engineering stress–strain curves of TRIP60 with the variation of the strain rate and the temperature: (a) –40ºC; (b) 20ºC; (c) 100ºC; (d) 200ºC.

show that the flow stresses of the SPRC35R, SPRC45E and TRIP60 steels are influenced not only by the environmental temperature but also by the strain rate. In order to clarify the effect of the strain rate on the deformation of these steels, the yield stresses are plotted in the logarithmic scale of the strain rate at temperatures of –40, 20, 100 and 200ºC as shown in Figure 6. The yield stress and the slop of the curves increase significantly with

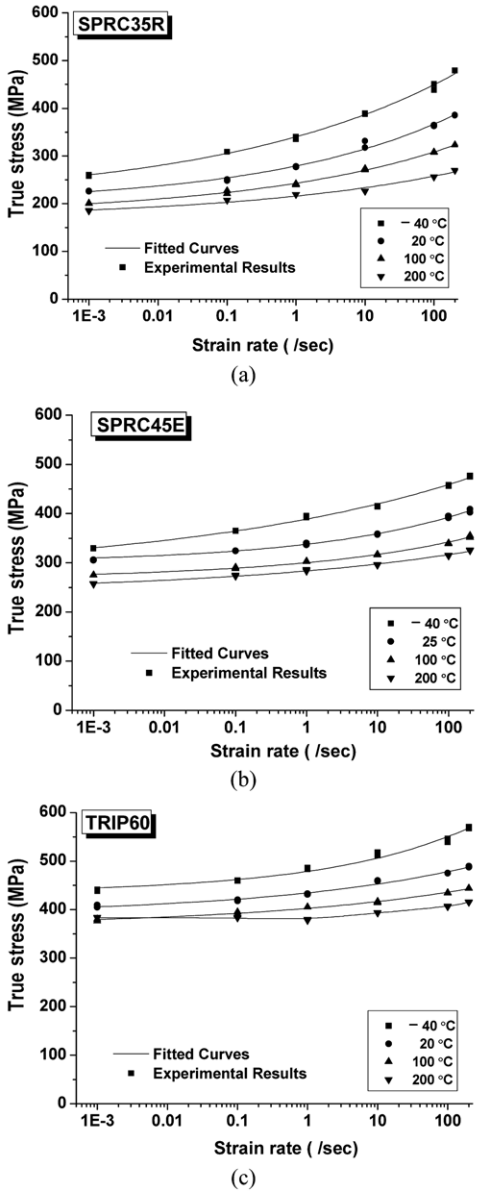

Figure 6. Variation of the yield stress with respect to the strain rates at corresponding temperatures: (a) SPRC35R; (b) SPRC45E; (c) TRIP60.

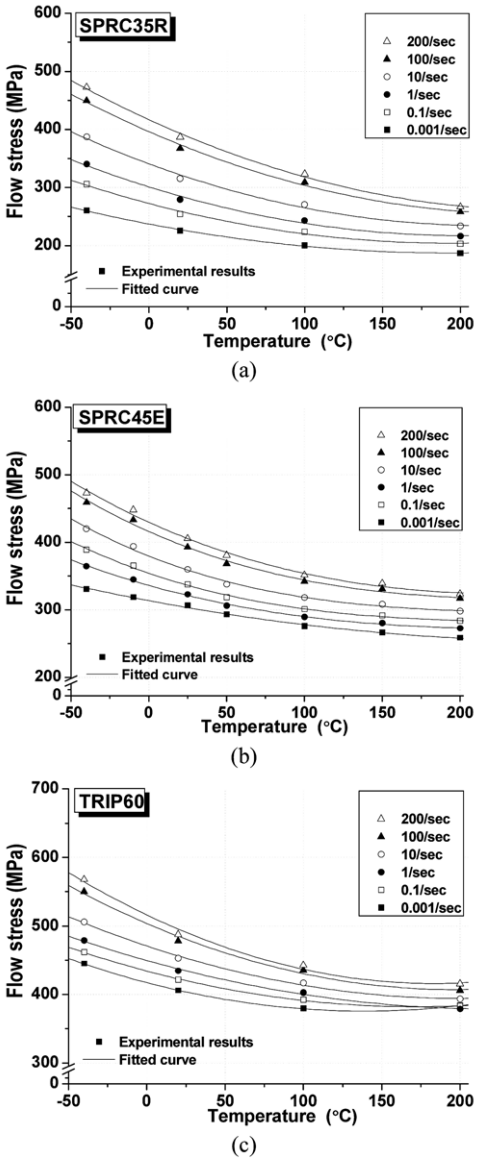

Figure 7. Variation of the yield stress with respect to the temperature at corresponding strain rates: (a) SPRC35R; (b) SPRC45E; (c) TRIP60.

increasing strain rates. The figures also represent that the slop of curves increases with decreasing temperature, which means that strain rate hardening has a more noticeable effect at the low temperature. Consequently, it is apparent that the strain-rate sensitivity of each steel decreases at a constant strain rate with increasing temperature, while it increases with increasing strain rate at a given temperature. The influence of the temperature is also investigated and depicted in Figure 7(a), (b) and (c) representing the variation of the yield stress for SPRC35R, SPRC45E and TRIP60 with respect to the temperature at the corresponding strain rates, respectively. For a constant strain rate, the yield stress decrease with increasing temperature. It is also observed that the amount of decrease in the yield stress is least at the strain rate of 0.001/sec when the temperature increases from –40°C to 200°C and increases as the strain rate increases. This tendency implies that the temperature sensitivity decreases with increasing temperature at a constant strain rate, while it increases with increasing strain rates at a given temperature.

In order to quantify the strain rate and the temperature effect on the flow stress, the value of the strain-rate sensitivity and the temperature sensitivity are defined as equation (1) and equation (2), respectively.

$$m = \frac{d(\ln\sigma)}{d(\ln\dot{\varepsilon})} \approx \frac{\Delta(\ln\sigma)}{\Delta(\ln\dot{\varepsilon})} \quad (1)$$

$$p = \left(\frac{d\sigma}{dT}\right) \approx \left(\frac{\Delta\sigma}{\Delta T}\right) \quad (2)$$

Table 2 and 3 summarize the variation of the strain-rate sensitivity and the temperature sensitivity including the flow stress increment. The negative value of the temperature sensitivity denotes the decrease of the flow stress with respect to the increase of the temperature. It could be confirmed that the strain-rate sensitivity decreases as the temperature increases while the temperature sensitivity increases as the strain rate increases. Table 2 and 3 also represent that the low strength steel such as SPRC35R is more sensitive to the strain rate and the temperature than the high strength steel such as SPRC45E and TRIP60.

3.2. Dynamic Strain Aging

The yield stress of SPRC35R and SPRC45E shows the positive strain-rate sensitivity over a range of intermediate strain rates and temperatures from –40°C to 200°C. On the other hand, the yield stress of TRIP60 has the positive strain-rate sensitivity over a range of temperatures from –40°C to 100°C, but the negative strain-rate sensitivity is observed at the temperature between 100°C and 200°C at the strain rate of 0.001/sec as shown in Figure 6(c) and Figure 7(c). Such behavior could be explained by dynamic strain aging which is the occurrence of aging during straining (Cottrell, 1953; McCormick, 1978; Li and Leslie, 1978; Robinson and Shaw, 1994). Its main effects, other than negative strain-rate sensitivity, are increasing strain hardening, decreases in ductility, and jerky flow.

In order to confirm the dynamic strain aging behavior of TRIP60, additional tensile tests were conducted at the temperature of 150°C and 250°C with the strain rate of 0.001/sec and 0.1/sec. Figure 8(a) shows the close view of stress–strain curve for TRIP60 at the strain rate 0.001/sec with the variation of temperature. The serrated flow is observed and both the flow stress and level of serration are increased with increasing temperature after 150°C. The phenomena of increasing the level of flow stress and serration with increasing temperature are evidences that dynamic strain aging takes place in TRIP60 at the temperature near 150°C. It is commonly accepted that the dynamic strain aging is related to the pinning of

Table 2. Strain rate sensitivity of SPRC35R, SPRC45E and TRIP60.

Material		0.001 /sec	0.1 /sec	1 /sec	10 /sec	100 /sec	200 /sec
SPRC 35R	Δσ (MPa)	–74	–103	–124	–154	–192	–206
	p	–0.31	–0.43	–0.52	–0.64	–0.80	–0.86
SPRC 45E	Δσ (MPa)	–72	–92	–105	–122	–143	–150
	p	–0.30	–0.38	–0.44	–0.51	–0.60	–0.62
TRIP 60	Δσ (MPa)	–61	–78	–100	–113	–144	–153
	p	–0.26	–0.33	–0.42	–0.47	–0.60	–0.64

Table 3. Temperature sensitivity of SPRC35R, SPRC45E and TRIP60.

Material		–40°C	20°C	100°C	200°C
SPRC35R	Δσ (MPa)	212	161	123	80
	m	0.049	0.044	0.039	0.029
SPRC45E	Δσ MPa)	142	99	75	64
	m	0.029	0.023	0.020	0.018
TRIP60	Δσ (MPa)	123	82	63	31
	m	0.020	0.016	0.013	0.007

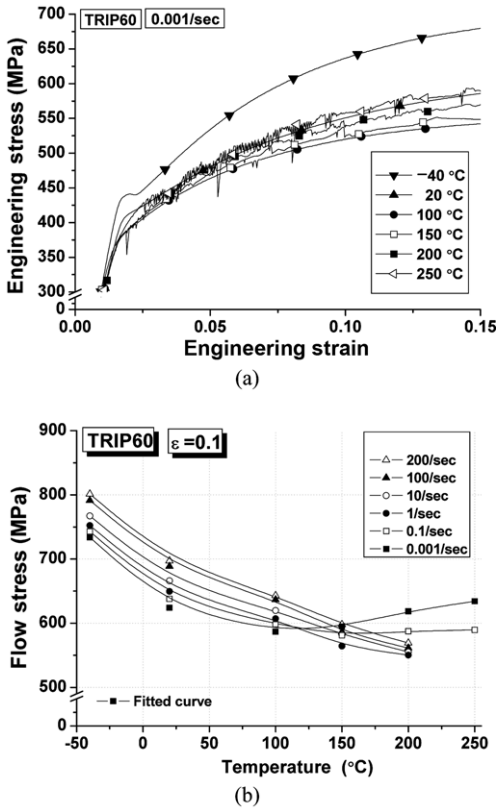

Figure 8. Dynamic strain aging of TRIP60: (a) Close view of engineering stress–strain curves; (b) variation of the flow stress with respect to the temperature.

dislocations by diffusing solute atoms such as C and N during the aging period and it has a significant influence on the material response of carbon steels at temperatures between 200°C~400°C (Gilat and Xu, 1997). Since the amount of carbon content in TRIP60 is higher than that in SPRC35R and SPRC45E as summarized in Table 1, the dynamic strain aging is observed only in TRIP60 at the relatively lower temperature.

Figure 8(b) depicts the variation of flow stress at the plastic strain of 0.1 with respect to the temperature at corresponding strain rates. Negative strain-rate sensitivity can be found at the temperature near the temperature of 150°C. As the strain rate increases from 0.001/sec to 0.1/sec, the tendency of increasing flow stress with increasing temperature becomes diminished. It is because that higher temperature is required to drive the solutes to dislocation at sufficient speeds as the strain rate increases. Consequently, it can be deduced that the dynamic strain aging temperatures are increased as the strain rate increases.

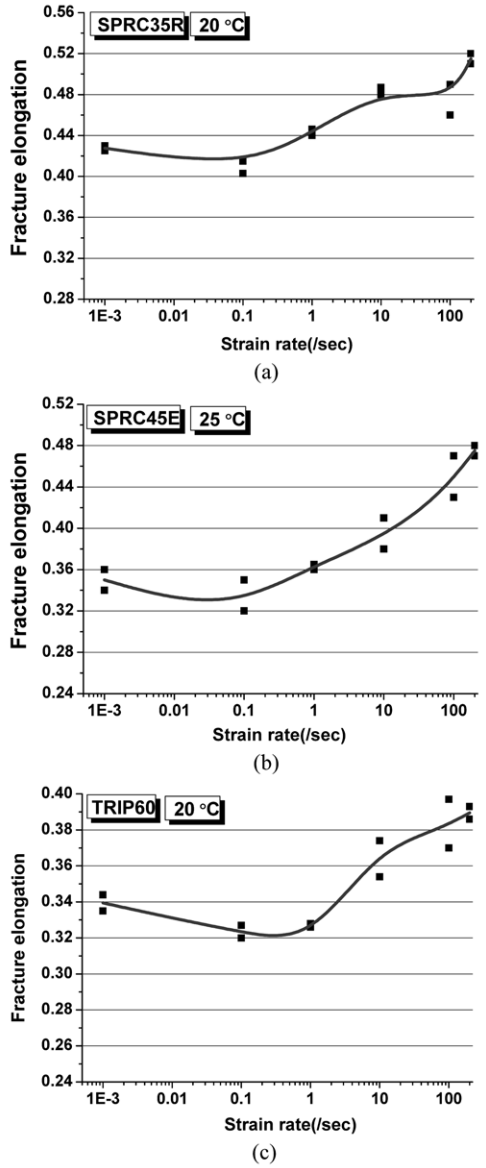

Figure 9. Variation of the fracture strain with respect to the strain rate at room temperature: (a) SPRC35R; (b) SPRC45E; (c) TRIP60.

3.3. Fracture Elongation

The fracture elongation was obtained from the engineering stress–strain curves at various strain rates and temperatures. Figure 9 shows the fracture elongation distribution with respect to the logarithmic scale of the strain rate at the room temperature. In the classical conjecture, the fracture elongation is expected to decrease as the strain rate increases. However, tensile test results show that the fracture elongation of SPRC35R, SPRC45E and TRIP60 tends to decrease at the strain rate from 0.001 to 0.1/sec at room temperature and then increase at the strain rate up to 100/sec. When the necking phenomenon occurs in simple static tensile tests, deformation is concentrated at the gauge region in a narrow band. On the other hand, in tensile tests at the high stain rate, local strain rate hardening restrains the progress of necking and elongation propagates in the adjacent region forming a wide band of necking. It is because the strain rate at the necking region becomes particularly higher than the other region and the flow stress in the necking region exceeds the flow stress in the other region due to the rapid increase of the strain rate. Consequently, the necking region becomes stronger than the neighboring region despite of the thinning in the necking region. Due to this phenomenon, fracture elongation increases as the strain rate increases.

In order to inspect the effect of temperature at a given strain rate, the fracture elongation distributions are plotted with respect to the variation of temperatures as shown in Figure 10. At the strain rate of 0.001/sec, which is regarded as a quasi-static state, the fracture elongation decreases as the temperature increases. The tendency that the decrease of the fracture elongation as increasing the temperature relates on the blue brittleness of a material due to dynamic strain aging. For carbon steels, fracture elongation generally decreases as increasing temperature up to 200°C~300°C, and then it increases as the temperature increases (Robinson and Shaw, 1994). However, as the strain rate increases above 0.1/sec, the fracture elongation tends to increase from –40°C to room temperature and then decrease at the temperature up to 200°C. Moreover, it could be seen that this increase of the fracture elongation at low temperature becomes more remarkable as the strain rate increases. This phenomenon seems to occur because of the high strain-rate sensitivity at low temperature which makes the necking region stronger than the neighboring region so that the necking is restricted to proceed at the neighboring region and rather spreads to the neighboring region. This experimental result is worthy of attention for the crashworthiness of an auto-body especially in terms of the

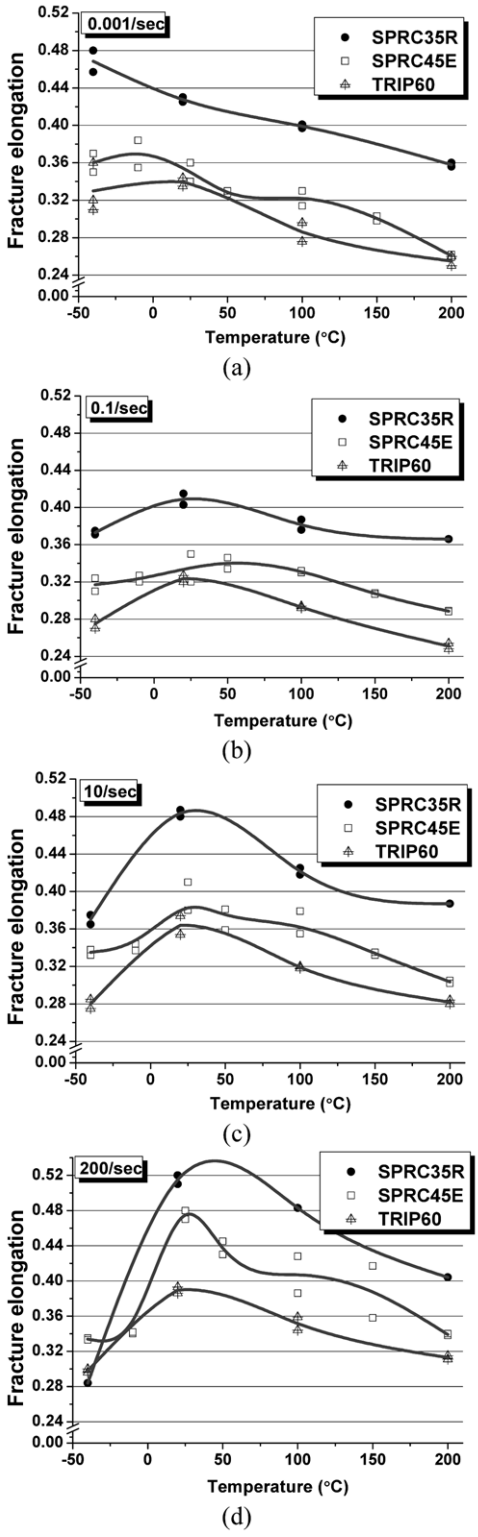

Figure 10. Variation of the fracture strain with respect to the temperature: (a) 0.001/sec; (b) 0.1/sec; (c) 10/sec; (d) 200/sec.

fracture and tearing of auto-body members. This result is also applicable to sheet metal forming processes of auto-body members in order to enhance the formability of sheet metals.

4. CONSTITUTIVE MODELING

The next important procedure is constructing a reliable description for application to real problems from experimental data for temperature-dependent dynamic behavior of steel sheets for an auto-body. An accurate physical and numerical modeling of the mechanical response is necessary for reliable simulation of structures. Considering both the strain rate and the temperature, several constitutive relationships have been proposed for metallic materials under impact loading for implementation in computational mechanics, which vary from being purely empirical to highly theoretical (Liang and Khan, 1999). The empirical models which are generally called as the phenomenological models are based on available experimental observations while the latter of so-called physically-based models are based on the microscopic nature such as the dislocation mechanism of materials. The physically-based models are so difficult to evaluate many material constants and to utilize in computational procedures in which the phenomenological models are widely utilized in the finite element crash simulation. The basic form of the phenomenological model is well suited for computations because the model defines variables that are readily available in most of the applicable computer codes. Most phenomenological models are, however, highly based on the experimental data obtained from the quasi-static test for the hardening curve and the Hopkinson bar test for scaling of the yield stress. Special cares should be taken for the variation of the hardening curve at the intermediate strain rates in order to apply the phenomenological model to the numerical simulation of the material deformation such as crushing deformation of an auto-body.

This paper focuses on the phenomenological modeling of the temperature-dependent hardening curve of steel sheets at intermediate strain rates. In order to confirm the validity of the well-known phenomenological model such as the Johnson–Cook model (Johnson and Cook, 1983) and the Khan–Huang–Liang model (Khan and Huang, 1992; Khan and Liang, 1999, 2000) at intermediate strain rates, hardening curves interpolated with both the Johnson–Cook and the Khan–Huang–Liang models are compared with those obtained from experiments at various strain rates and temperatures. The assessment of validation shows that there are some discrepancy between the interpolated stress–strain curves and experimental ones. This result claims necessity of a new phenomenological constitutive relationship which should be proposed based on the material behavior observed over a range of intermediate strain rates from 0.001/sec to 200/sec and temperatures from –40°C to 200°C.

4.1. Johnson–Cook Model

Johnson and Cook (Johnson and Cook, 1983) proposed a phenomenological constitutive model which has been frequently used in the impact analysis due to its simplicity. The Johnson–Cook model can be stated as:

$$\sigma = (A + B\varepsilon^{n})\left(1 + C\ln\left(\frac{\dot{\varepsilon}}{\dot{\varepsilon}_0}\right)\right)(1 - T^{*m}) \tag{3}$$

where ε is the equivalent plastic strain, $\dot{\varepsilon}$ is the equivalent strain rate, $\dot{\varepsilon}_0$ is the reference stain rate normally taken to be 1.0/sec, and T^* is the homologous temperature represented by equation (4):

$$T^* = \frac{T - T_{room}}{T_{melt} - T_{room}} \tag{4}$$

where T is the current temperature and T_{melt} is the melting temperature of the specimen.

The first bracketed term in the Johnson–Cook model is the strain hardening term; the second is the strain rate hardening term; and the third is the thermal softening term. The Johnson–Cook model interpolates the initial yield stress at the strain rate of 1/sec and higher levels as a linear function with the logarithm of strain rate. In order to verify the validity of the Johnson–Cook model at intermediate strain rates, five material constants in the equation (3) are determined using the experimental data. Figure 11 represents that the comparison of the flow stress curves at various strain rates and temperatures for SPRC45E between the interpolated results with both the Johnson–Cook model and the experimental data. The solid symbol and line represents the experimental data while the hollow symbol and line denotes the interpolated one. The comparison indicates that there are some discrepancy between the interpolated hardening curves and experimental ones. It is because that the Johnson–Cook model interpolates the stress-strain curves at the strain rate of 1/sec and scales the subsequent stress–strain curves only with a linear function of the yield stress with respect to the logarithmic scale of strain rate while the flow stress is exponentially increased with the logarithmic scale of the strain rate as the strain rate increases. The Johnson–Cook model does not describe the rate-dependent hardening characteristics which is identified as the decrease of the work-hardening rate with increasing strain rate as frequently observed for most steel sheets at intermediate strain rates.

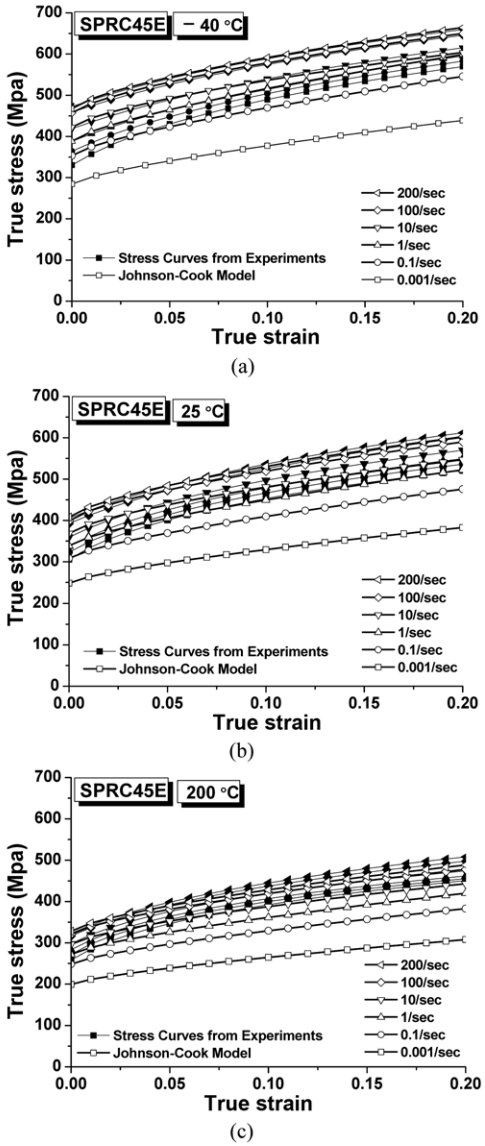

Figure 11. Comparison of the flow stress between interpolated with the Johnson–Cook model and obtained with the experiment for SPRC45E: (a) –40ºC; (b) 25ºC; (c) 200ºC.

4.2. Khan–Huang–Liang Model

A simple multiplication form of the Johnson–Cook model has an inherent problem of modeling the description of the strain-hardening behavior of materials with strain rate and temperature dependence. Base on the experimental data, a new constitutive model named as the Khan–Huang–Liang model was proposed by considering the coupled effect of the strain and the strain rate on the description of the work-hardening relation (Khan and Huang, 1992; Khan and Liang, 1999, 2000). The Khan–Huang–Liang model is expressed as:

$$\overline{\sigma} = \left(A + B\left(1 - \frac{\ln\dot{\varepsilon}}{\ln D_0^P}\right)^{n_1}\varepsilon^{n_0}\right)e^{C\ln\dot{\varepsilon}}(1 - T^{*m}) \tag{5}$$

where D_0^P is chosen to be 10^6 /sec, and T^* is the homologous temperature represented by equation (4).

The Khan–Huang–Liang model is similar to the Johnson–Cook constitutive equation, but here the work-hardening is dependent on the strain rate so that decreasing work-hardening with increasing strain rate can be

accommodated by modifying the Ludwick hardening equation in the first bracket. The Khan–Huang–Liang model interpolates the logarithm of the initial yield stress as a linear function of the logarithm of the strain rate.

In order to investigate the accuracy of interpolation with the Khan–Huang–Liang model at intermediate strain rates, six material constants in the equation (5) are determined using the experimental data for SPRC45E and flow stress curves at various strain rates and temperatures interpolated with the Khan–Huang–Liang model are compared with real data obtained from the experiment. The comparison depicted in Figure 12 represents that the discrepancy still exists especially at the low strain rates and with the

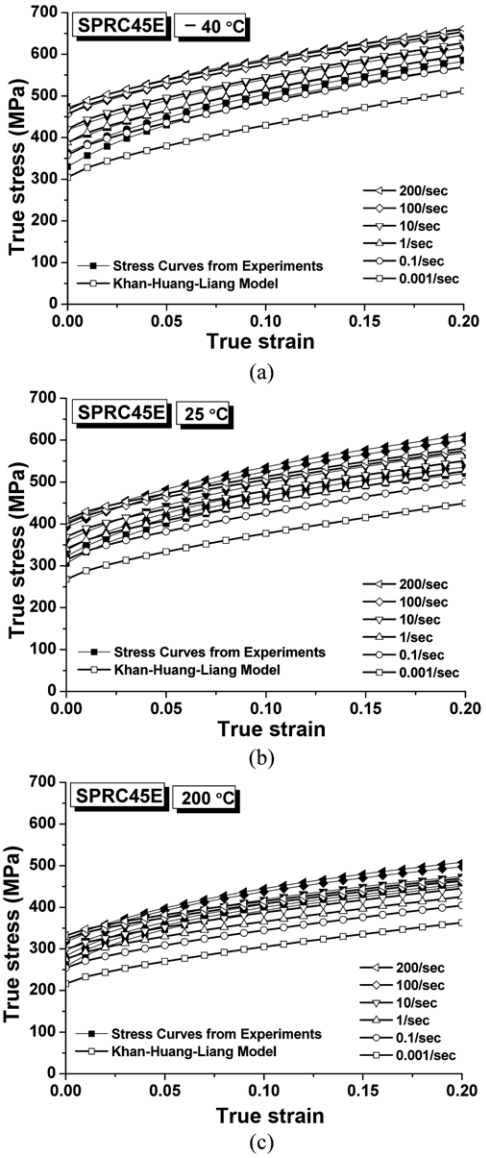

Figure 12. Comparison of the flow stress between interpolated with the Khan–Huang–Liang model and obtained with the experiment for SPRC45E: (a) –40°C; (b) 25°C; (c) 200°C.

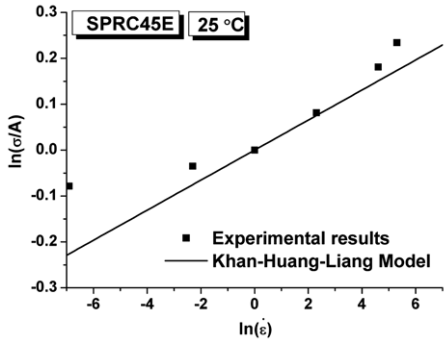

Figure 13. Description of initial yield stress with respect to the strain rate for SPRC45E at room temperature using the Khan–Huang–Liang model.

variation of temperatures although the Khan–Huang–Liang model describes the experimental response closer than the Johnson–Cook model by accounting for the strain rate effect on the work-hardening characteristics. Figure 13 represents the determination of the material constant C which implies the strain-rate sensitivity of the flow stress for SPRC45E in the Khan–Huang–Liang model. The figure reveals that the linear interpolation of the logarithmic scale of the yield stress with respect to the logarithmic scale of the strain rate comprises the inadequate prediction of the strain-rate sensitivity at low and intermediate strain rates. The comparison also indicates that the strain-rate dependent thermal-softening behavior has to be carefully counted in the constitutive model to reduce the discrepancy between the interpolation and the experiment within overall testing temperatures.

4.3. Modification of the Khan–Huang–Liang Model

The assessment of validation of the Johnson–Cook and the Khan–Huang–Liang models shows that phenomenological constitutive models established so far have some problems to describe the material behavior of steel sheets with various temperatures at intermediate strain rates. The experimental observation indicates that the strain-rate sensitivity of steel sheets decreases at a constant strain rate with increasing temperature while it increases with increasing strain rate at a given temperature. It is also apparent that the temperature sensitivity decreases with increasing temperature at a constant strain rate while it increases with increasing strain rates at a given temperature. It is concluded from experimental results that not only the strain and the strain rate but also the temperature should be coupled on the description of the work-hardening behavior of steel sheets for better interpolation.

In this reason, a new phenomenological constitutive relationship is proposed based on the experimental data. The Khan–Huang–Liang model can describe the decrease

of the work-hardening rate with increasing strain rate, which is important characteristics for most steel sheets at intermediate strain rates (Huh *et al*., 2009). However, the Khan–Huang–Liang model interpolates the flow stress inadequately at the low strain rates and with the variation of temperatures. Developing a new model focuses on accepting the merits of the Khan–Huang–Liang model and modifying it to consider the hardening characteristics dependent on both the strain rate and the temperature.

A modified Khan–Huang–Liang model is represented by equation (6).

$$\bar{\sigma} = \left(A + B\left(1 - \frac{\ln \dot{\varepsilon}^*}{\ln D_0^{p_0}}\right)^{n_1} \varepsilon^{n_0}\right)(1 + C(\ln \dot{\varepsilon}^*)^P)(1 - T^{*m}) \tag{6}$$

where $\dot{\varepsilon}^* = \dot{\varepsilon}/\dot{\varepsilon}_{\text{ref}}$, and $\dot{\varepsilon}_{\text{ref}}$ is the reference strain rate. The strain rate is normalized with the reference strain rate at which the quasi-static test is performed and the strain rate hardening term in the second bracket is modified with an exponential function of the logarithm of the normalized strain rate in order to accommodate an inaccurate interpolation at low and intermediate strain rates. Figure 14(a) represents the interpolation of the yield stress of SPRC45E with respect to the logarithmic scale of the strain rates using the modified Khan–Huang–Liang model. The figure indicates that the exponential function of the normalized strain rate in the present model interpolates the flow stress accurately compared with the linear function in the Khan–Huang–Liang model.

In order to consider the temperature-dependent strain-rate sensitivity and the strain-rate dependent temperature sensitivity for the constitutive model, the variation of the coefficient of n1 which implies the rate-dependent hardening behavior is plotted with the variation of the temperature as shown in Figure 14(b) and the variation of the coefficient of m which is related to the temperature sensitivity is also figured with the variation of the strain rate as shown in Figure 14(c). And then the coefficients of n1 and m are assigned as a function of the temperature and the strain rate respectively as represented by equation (7) and (8):

$$n_1 = a \cdot (1 - T^{*b}) \tag{7}$$

$$m = m_1 + m_2 \cdot \ln \dot{\varepsilon} \tag{8}$$

so that the flow stress is consequently coupled with the strain, the strain rate and the temperature. From the above procedure, the modified Khan Huang–Liang model is expressed as follows:

$$\bar{\sigma} = \left(A + B\left(1 - \frac{\ln \dot{\varepsilon}^*}{\ln D_0^{p_0}}\right)^{n_1} \varepsilon^{n_0}\right)(1 + C(\ln \dot{\varepsilon}^*)^P)(1 - T^{*m}) \tag{9}$$

where $\dot{\varepsilon}^* = \dot{\varepsilon}/\dot{\varepsilon}_{\text{ref}}$, $n_1 = a \cdot (1 - T^{*b})$ and $m = m_1 + m_2 \cdot \ln \dot{\varepsilon}$.

The material constants of the proposed model have some physical meaning. A is the yield stress at the quasi-static state; B and n_0 is the work-hardening at the quasi-static strain rate; C and p is the coefficient of the strain rate hardening; a and b is the change of work-hardening rate with respect to the temperature and m_1 and m_2 is the strain-rate dependent thermal softening, respectively.

The material constants of SPRC45E are determined using the experimental data. Flow stress curves of SPRC45E interpolated with the modified Khan–Huang–Liang model are compared with those obtained from the

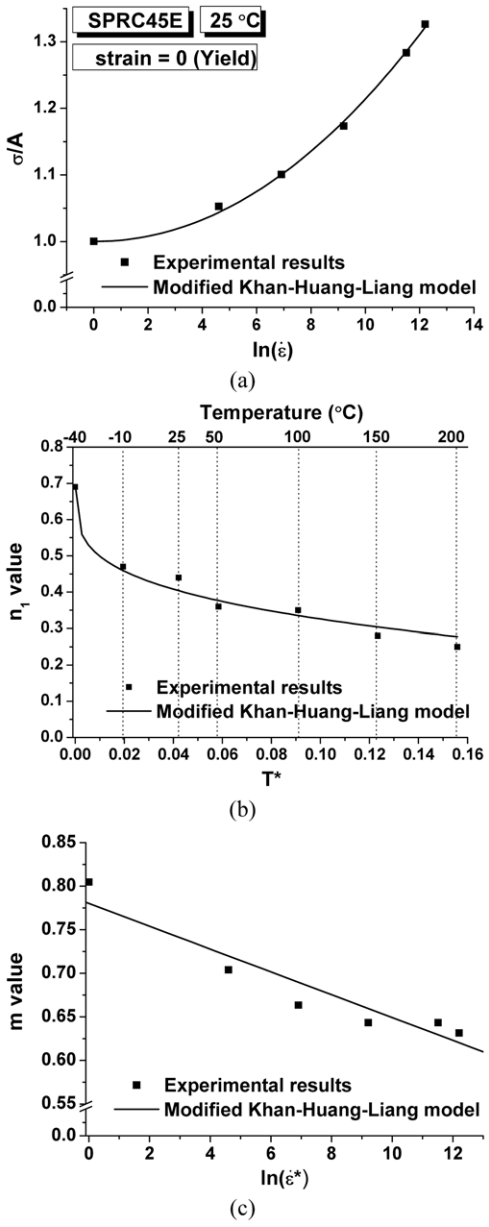

Figure 14. Determination of material constants for SPRC45E using the modified Khan–Huang–Liang model: (a) strain rate sensitivity; (b) fitting of n_1 vs. T^*; (c) fitting of m vs. $\ln \dot{\varepsilon}$.

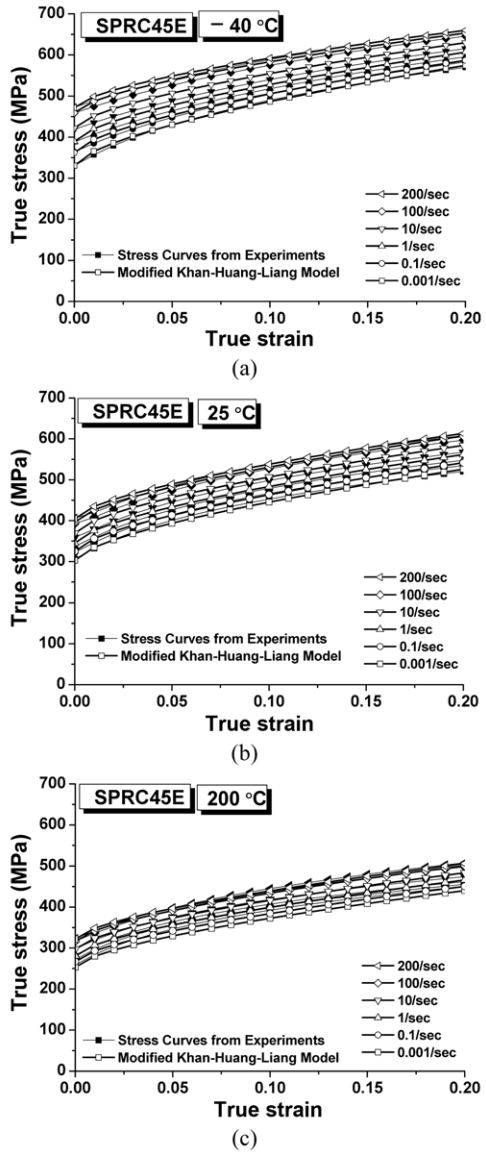

Figure 15. Comparison of the flow stress between interpolated with the modified Khan–Huang–Liang model and obtained with the experiment for SPRC45E: (a) –40°C; (b) 25°C; (c) 200°C.

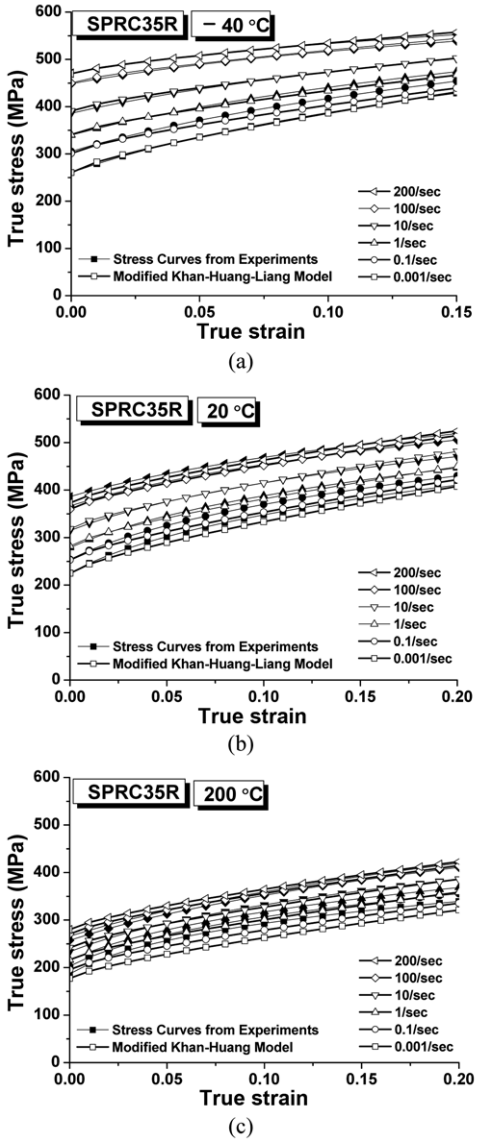

Figure 16. Comparison of the flow stress between interpolated with the modified Khan–Huang–Liang model and obtained with the experiment for SPRC35R: (a) –40°C; (b) 20°C; (c) 200°C.

experiment as shown in Figure 15. Similar comparisons are also performed for SPRC 35R and TRIP60 as shown in Figure 16 and Figure 17, respectively. The hardening equation of TRIP60 is constructed with only the seven material constants without loss of accuracy since the flow stress of TRIP60 is less sensitive to the strain rate and the temperature. The figures represent that the constitutive model proposed gives relatively good correlation with the experimental data of steel sheets at various intermediate strain rates and temperatures. The material constants of steel sheets for the modified Khan–Huang–Liang model are listed in the Table 4.

In order to compare the interpolation accuracy of the proposed model qualitatively, the interpolated stress–temperature curves at various designated strain rates are compared with the experimental data for a fixed strain of 10% as shown in Figure 18. It can be seen that the Johnson–Cook and Khan–Huang–Liang models provide inadequate predictions at the low strain rate of 0.001/sec and become less accurate with increasing temperature at the strain rate of 200/sec. It is because the primary applications of the Johnson–Cook and the Khan–Huang–Liang models are deformation of materials at higher strain

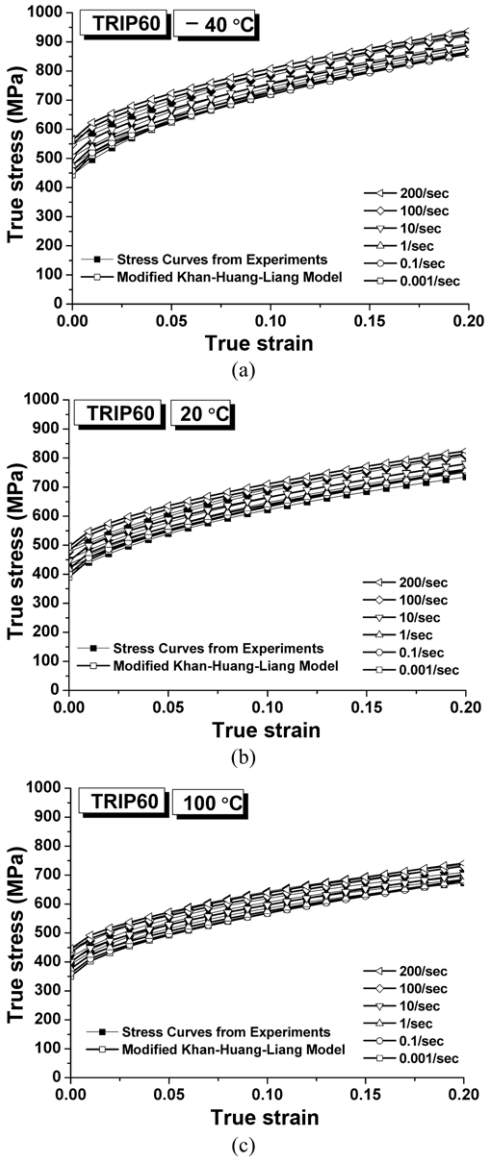

Figure 17. Comparison of the flow stress between interpolated with the modified Khan–Huang–Liang model and obtained with the experiment for TRIP60: (a) –40°C; (b) 20°C; (c) 100°C.

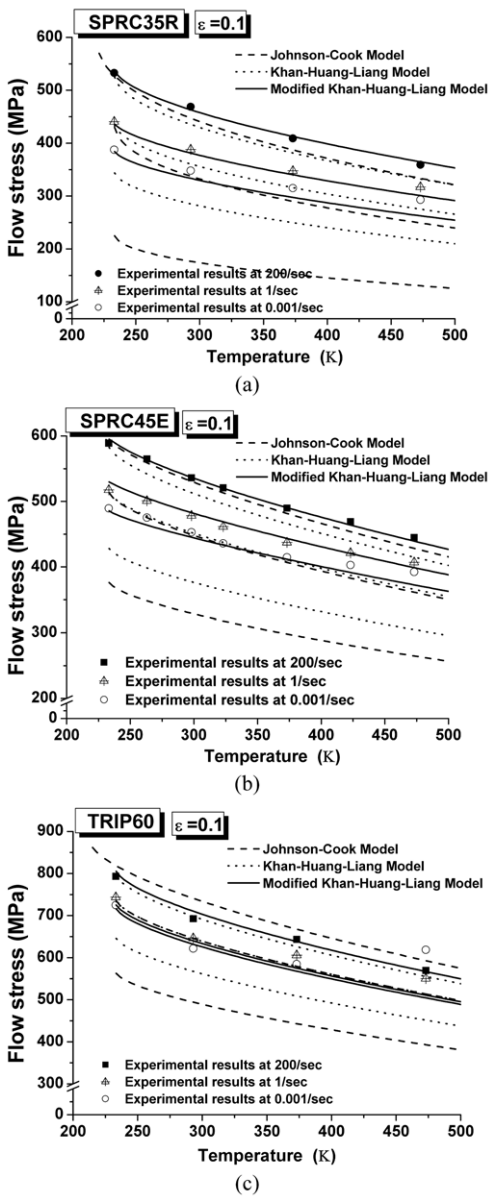

Figure 18. Comparison of the constitutive models with experimental results at the strain of 10% with various strain rates and temperatures: (a) SPRC35R; (b) SPRC45E; (c) TRIP60.

rates and thus linear interpolation with the logarithmic scale of the strain rate is adopted for describing the strain rate hardening. On the other hand, the modified Khan–Huang–Liang model gives a relatively better prediction over a wide range of intermediate strain rates and temperatures since the proposed model interpolates the strain rate hardening with the exponential function of the logarithm of the strain rate and the coupled effect of the strain rate and the temperature on the flow stress are also taken into account. For the quantitative assessment of the present model, the standard error (Stevenson, 1982) between the interpolated result and the experimental one is compared with those of the Johnson–Cook and the Khan–Huang–Liang models. Figure 19 shows the standard error for SPRC35R with the variation of the strain rate and the temperature. Figure 20 and Figure 21 also represent the standard error for SPRC45E and TRIP60 respectively. The modified Khan–Huang–Liang model provides the maximum standard error of 3 MPa for SPRC45E while the Johnson–Cook and the Khan–Huang–Liang models produce the maximum error of 27 MPa and 20 MPa, respectively. These qualitative and quantitative comparisons fully demonstrate

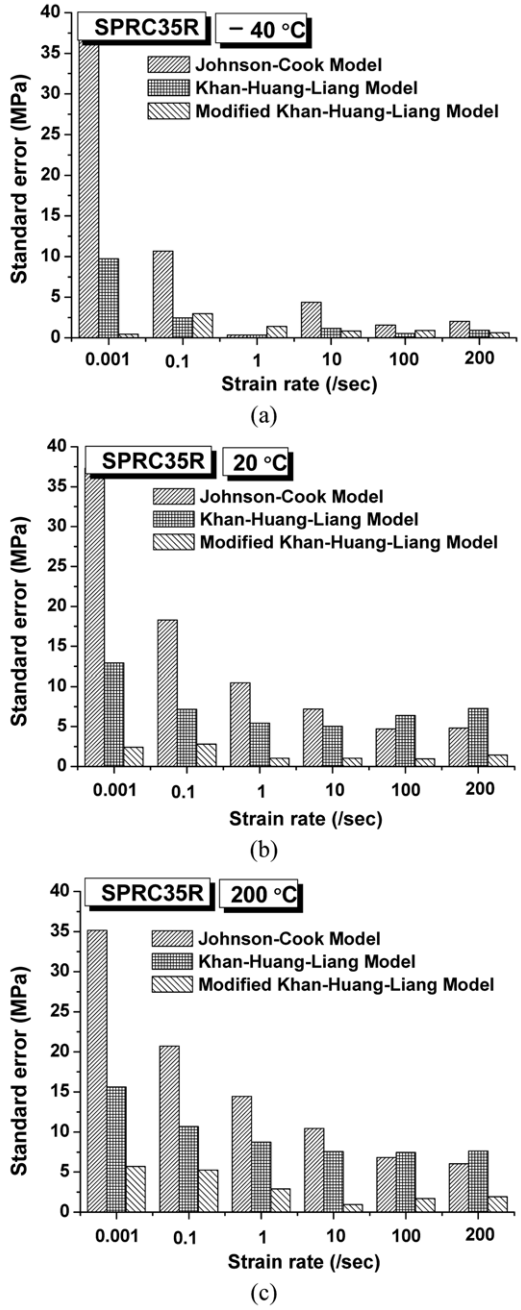

Figure 19. Comparison of the standard error for SPRC35R with respect to constitutive models: (a) –40ºC; (b) 20ºC; (c) 200ºC.

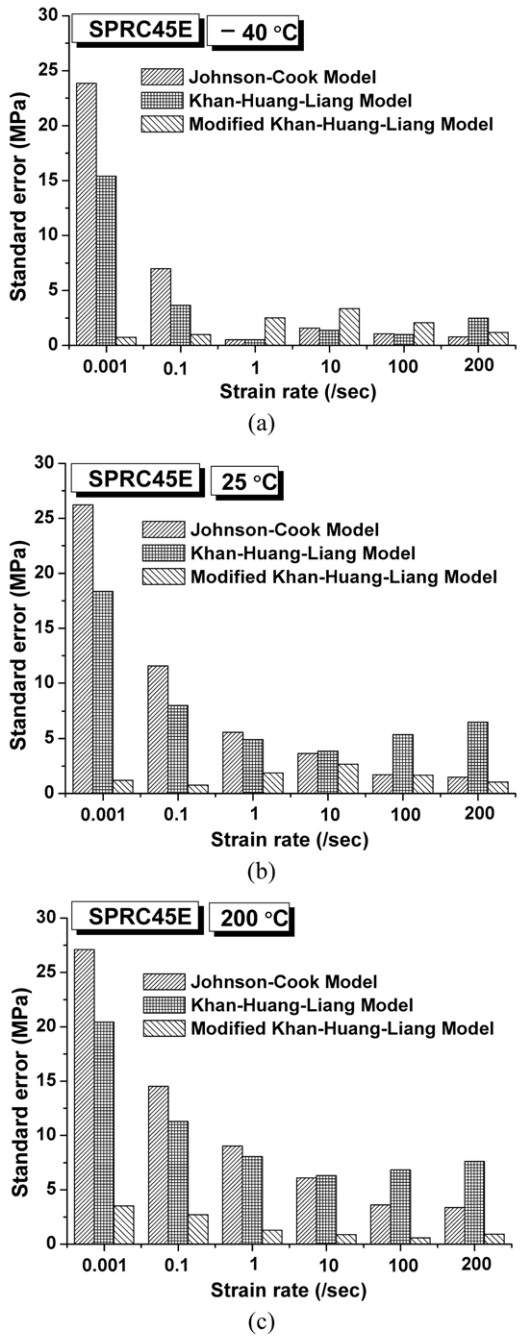

Figure 20. Comparison of the standard error for SPRC45E with respect to constitutive models: (a) –40ºC; (b) 25ºC; (c) 200ºC.

that the present model gives well description of experimental data at intermediate strain rates with various temperatures.

5. CONCLUSION

This paper proposes a new empirical hardening equation of steel sheets for an auto-body at the intermediate strain rate with the variation of temperature as a modification of the Khan–Huang–Liang model. The constitutive model proposed is constructed based on the experimental data in order to consider the hardening characteristics dependent on both the strain rate and the temperature. The model reveals unusual temperature dependence of the strain-rate

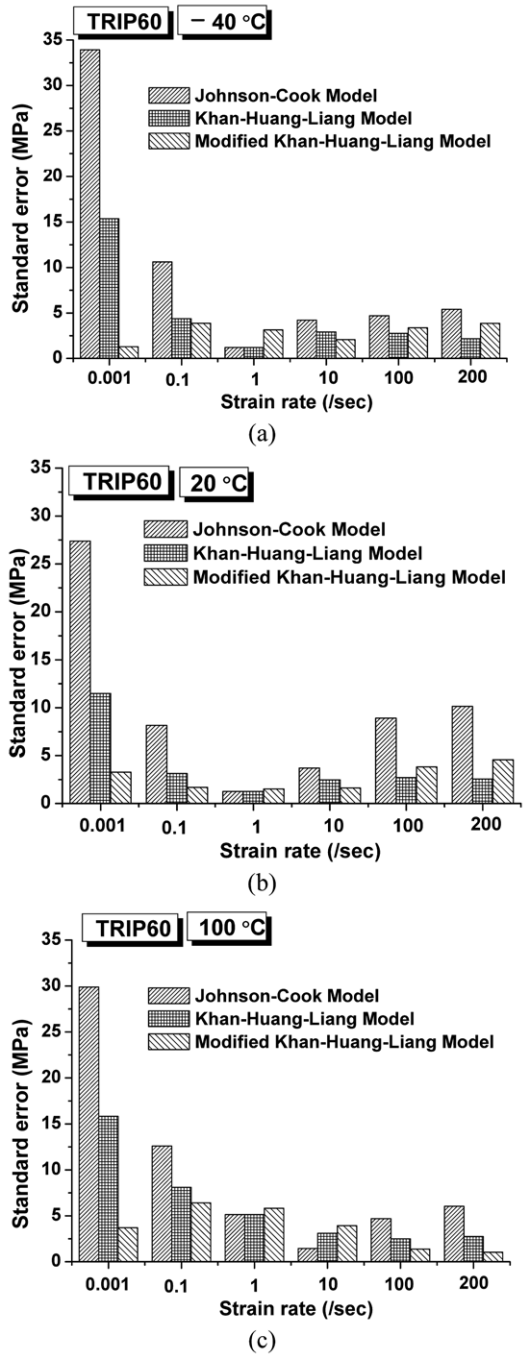

Figure 21. Comparison of the standard error for TRIP60 with respect to constitutive models: (a) –40°C; (b) 20°C; (c) 100°C.

sensitivity of steel sheets such as SPRC35R, SPRC45E and TRIP60 at the intermediate strain rate. The conclusions are summarized as follows:

(1) A constitutive model is newly proposed to describe the hardening characteristics dependent on both the strain rate and the temperature. In the hardening equation proposed, the strain-rate sensitivity is expressed with an exponent function of the logarithm of the normalized strain rate. The coefficients for the rate-dependent hardening behavior and the temperature sensitivity are assigned as a function of the temperature and the strain rate so that the flow stress is consequently coupled with the strain, the strain rate and the temperature. Qualitative and quantitative assessment fully demonstrates that the present model gives well description of experimental data at intermediate strain rates and various temperatures.

(2) The strain-rate sensitivity of steel sheets decreases with increasing temperature at a constant strain rate while it increases with increasing strain rate at a given temperature. The temperature sensitivity decreases with increasing temperature at a constant strain rate while it increases with increasing strain rates at a given temperature.

(3) Low strength steel such as SPRC35R is more sensitive to the strain rate and the temperature than the high strength steel such as SPRC45E and TRIP60.

(4) At the quasi-static state, negative strain-rate sensitivity is observed for TRIP60 at the temperature near 150°C due to the dynamic strain aging. As the strain rate increases, dynamic strain aging tends to take place at a higher temperature than 150°C.

(5) At the quasi-static state, the fracture elongation decreases as the temperature increases. However, as the strain rate increases above 0.1/sec, the fracture elongation tends to increase from –40°C to room temperature and then decrease at the temperature up to 200°C. Moreover, this increase of the fracture elongation at low temperature becomes more remarkable as the strain rate increases.

Table 4. Material constants of steel sheets for the modified Khan-Huang model

	A	B	n_0	q_1	q_2
SPRC35R	260.53	709.09	0.75	1.41	0.25
SPRC45E	330.35	691.18	0.65	0.69	0.27
TRIP60	443.69	1135.3	0.61	0.40	–
	C	p	m_1	m_2	
SPRC35R	0.0119	1.68	0.61	–0.0104	
SPRC45E	0.0091	1.54	0.78	–0.0135	
TRIP60	0.0009	2.27	0.65	–	

REFERENCES

Abed, F. H. and Voyiadjis, G. Z. (2005). Plastic deformation modeling of AL-6XN stainless steel at low and high strain rates and temperatures using a combination of bcc and fcc mechanism of metals. *Int. J. Plasticity*, **21**, 1618–1639.

Campbell, J. D. and Ferguson, W. G. (1970). The temperature and strain-rate dependence of the shear strength of mild steel. *Phil. Mag*., **21**, 63–82.

Costin, L. S., Crisman, E. E., Hawley, R. H. and Duffy, J. (1979). On the localization of plastic flow in mild steel tubes under dynamic torsional loading. In Mechanical Properties at High Rates of Strain, Edn J. Harding, *Inst. Phys. Conf. Ser. No.* 47, 90–100.

Cottrell, A. H. (1953). *Dislocations and Plastic Flow in Crystals*. Clarendon. Oxford.

Cowper, G. R. and Symonds, P. S. (1957). Strain hardening and strain-rate effects in the impact loading of cantilever beams. *Brown University Division of Applied Mathematics*. Report No. 28.

Eleiche, A. M. (1981). Strain rate history and temperature effects on the torsional-shear behavior of a mild steel. *Exp. Mech.*, **21**, 285–294.

Follansbee, P. S. and Kocks, U. F. (1988). A constitutive description of the deformation of copper based on the use of the mechanical threshold stress as an internal state variable. *Acta Metall*., **36**, 81–93.

Gilat, A. and Wu, X. (1997). Plastic deformation of 1020 steel over a wide range of strain rates and temperatures. *Int. J. Plasticity*, **13**, 611–632.

Hoge, K. J. and Mukherjee, A. K. (1977). Temperature and strain rate dependence of the flow stress of tantalum. *J. Mater. Sci.* **12**, **8**, 1666–1672.

Huh, H. and Kang, W. J. (2002). Crash-worthiness assessment of thin-walled structures with the high-strength steel sheet. *Int. J. Vehicle Des.*, **30**, 1–21.

Huh, H., Kang, W. J. and Han, S. S. (2002). A tension split Hopkinson bar for investigating the dynamic behavior of sheet metals. *Exp. Mech.*, **42**, 8–17.

Huh, H., Lim, J. H., Song, J. H., Lee, K. S., Lee, Y. W. and Han, S. S. (2003). Crashworthiness assessment of side impact of an auto-body with 60TRIP steel for side members. *Int. J. Automotive Technology* **4**, **3**, 149–156.

Huh, H., Kim, S. B., Song, J. H. and Lim, J. H. (2008). Dynamic tensile characteristics of TRIP-type and DP-type steel sheets for an auto-body. *Int. J. Mech. Sci.*, **50**, 918–931.

Huh, H., Lim, J. H. and Park, S. H. (2009). High speed tensile test of steel sheets for the stress-strain curve at the intermediate strain rate. *Int. J. Automotive Technology* **10**, **2**, 195–204.

Ishikawa, K. and Tanimura, S. (1992). Strain rate sensitivity of flow stress at low temperatures in 304N stainless steel. *Int. J. Plasticity*, **8**, 947–958.

Johnson, G. R. and Cook, W. H. (1983). A constitutive model and data for metals subjected to large strain, high strain rates and high temperatures. *Proc. 7th Int. Symp. Ballistics*, *The Hague, The Netherlands*, 541–547.

Kang, W. J., Cho, S. S., Huh, H. and Chung, D. T. (1999). Modified Johnson–Cook model for vehicle body crashworthiness simulation. *Int. J. Vehicle Des.*, **21**, 424–435.

Khan, A. S. and Liang, R. (1999). Behaviors of three BCC metal over a wide range of strain rates and temperatures: Experiments and modeling. *Int. J. Plasticity*, **15**, 1089–1109.

Khan, A. S. and Liang, R. (2000). Behaviors of three BCC metals during non-proportional multi-axial loadings: Experiments and modeling. *Int. J. Plasticity*, **16**, 1443–1458.

Khan, A. S. and Huang, S. (1992). Experimental and theoretical study of mechanical behavior of 1100 aluminum in the strain rate range 10^{-5}–10^{4} s^{-1}. *Int. J. Plasticity*, **8**, 397–424.

Khan, A. S., Suh, Y. S. and Kazmi, R. (2004). Quasi-static and dynamic loading responses and constitutive modeling of titanium alloys. *Int. J. Plasticity*, **20**, 2233–2248.

Khan, A. S. and Zhang, H. (2000). Mechanically alloyed nanocrystalline iron and copper mixture: Behavior and constitutive modeling over a wide range of strain rates. *Int. J. Plasticity*, **16**, 1477–1492.

Kim, J. S., Huh, H., Lee, K. W., Ha, D. Y., Yeo, T. J. and Park, S. J. (2006). Evaluation of dynamic tensile characteristics of polypropylene with temperature variation. *Int. J. Automotive Technology* **7**, **5**, 571–577.

Kim, K. P. and Huh, H. (2006). Dynamic limit analysis formulation for impact simulation of structural members. *Int. J. Solids Struct.*, **43**, 6488–6501.

Klepaczko, J. and Duffy, J. (1982). Strain rate history effects in body-centered-cubic metals. In Mechanical Testing for Deformation Model Development, Edn. R. W. Rhode and J. C. Swearengen, *ASTM STP765*, 251–268.

Kolsky, H. (1949). *Stress Wave in Solids*. Dover. New York.

Lee, W.-S. and Liu, C.-Y. (2006). The effects of temperature and strain rate on the dynamic flow behavior of different steels. *Mat. Sci. Eng. A*, **426**, 101–113.

Li, C. C. and Leslie, W. C. (1978). Effect of dynamic strain aging on the subsequent mechanical properties of carbon steels. *Metall. Trans.* A, **9**, 1765–1775.

Liang, R. and Khan, A. S. (1999). A critical review of experimental results and constitutive models for BCC and FCC metals over a wide range of strain rates and temperatures. *Int. J. Plasticity*, **15**, 963–980.

Mahadevan, K., McCoy, R., Schell, B. and Fekete, J. (1998). Strain-rate characterization of automotive steel and the effect of strain-rate in component crash analysis. *SAE Paper No*. 982392.

McCormick, P. G. (1978). Strain rate sensitivity prior to the onset of serrated yielding in a pressurized low carbon steel. *Scripta Metall.*, **12**, 197–208.

Meyers, A. (1994). *Dynamic Behavior of Materials*. John Wiley & Sons. New York.

Miura, K., Takagi, S., Obara, T. and Tanimura, S. (1996). Dynamic deformation behavior of steel sheet for automobile. *SAE Paper No*. 960019.

Nemat-Nasser, S. and Guo, W.-G. (2001). Thermomechanical response of AL-6XN stainless steel over a wide range of strain rates and temperatures. *J. Mech. Phys. Solids*, **35**, 1823–1846.

Nemat-Nasser, S. and Guo, W.-G. (2003). Thermomechanical response of DH-36 structural steel over a wide range of strain rates and temperatures. *Mech. Mater.*, **35**, 1023–1047.

Nemat-Nasser, S., Guo, W. G. and Kihl, D. P. (2001). Thermomechanical response of AL-6XN stainless steel over a wide range of strain rates and temperatures. *J. Mech. Phys. Solids*, **49**, 1823–1846.

Nemat-Nasser, S. and Isaacs, J. B. (1996). Direct measurement of isothermal flow stress of metals at elevated temperatures and high strain rates with application to Ta and Ta–W alloys. *Acta Mater.*, **45**, 907–919.

Porsche Engineering Service Inc. (2001). ULSAB-AVC Engineering Report.

Robert, A. A. (1983). Thermal gradients, strain rate and ductility in sheet steel tensile specimens. *Metall. Trans.* A, **16**, 37–43.

Robinson, J. M. and Shaw, M. P. (1994). Microstructural and mechanical influences on dynamic strain aging phenomena. *Int. Mater. Rev.*, **39**, 113–122.

Shi, N. F. and Meuleman, D. J. (1992). Strain rate sensitivity of automotive steels. *SAE Paper No*. 922045.

Song, J. H., Huh, H., Kim, H. G. and Park, S. H. (2006). Evaluation of the finite element modeling of a spot welded region for crash analysis. *Int. J. Automotive Technology* **7**, **3**, 329–336.

Stevenson, R. (1982). Inferring microscopic deformation behavior from the form of constitutive equation for low-carbon steel and 5182-0 aluminum. Edn R. W. Rhode and J. C. Swearengen, *ASTM STP*765, 366–381.

Tateno, H., Hishida, Y. and Shibata, K. (1998). New materials technology for achieving both crashworthiness and weight reduction using energy-absorbing steel with higher strain-rate sensitivity. *SAE Paper No*. 980953.

Uenishi, A. and Teodosiu, C. (2004). Constitutive modeling of the high strain rate behavior of interstitial-free steel. *Int. J. Plasticity*, **20**, 915–936.

Yasuki, T. (2000). An investigation on vehicle crash analysis accuracy. *Proc. EUROPAM 2000*, Nantes, France, 1–5.

Zener, C. and Holloman, J. H. (1944). Effect of strain rate upon plastic flow of steel. *J. Appl. Phys.*, **15**, 22–32.

Zerilli, F. J. and Armstrong, R. W. (1987). Dislocation-mechanics-based constitutive relations for material dynamics calculations. *J. Appl. Phys.*, **61**, 1816–1825.

Zukas, J. A., Nicholas, T., Swift, H. F., Greszczuk, L. B. and Curran, D. R. (1982). *Impact Dynamics*. John Wiley & Sons. New York.